






Open Archive Toulouse Archive Ouverte (OATAO)

OATAO is an open access repository that collects the work of Toulouse researchers and makes it freely available over the web where possible

This is an author's version published in: <http://oatao.univ-toulouse.fr/23377>

Official URL: <https://doi.org/10.1016/j.clay.2019.02.023>

To cite this version:

Lakbita, Omar  and Rhouta, Benaïssa and Maury, Francis  and Senocq, François  and Amjoud, M'barek and Daoudi, Lahcen *On the key role of the surface of palygorskite nanofibers in the stabilization of hexagonal metastable β -Ag₂CO₃ phase in palygorskite-based nanocomposites.* (2019) *Applied Clay Science*, 172. 123-134. ISSN 0169-1317

Any correspondence concerning this service should be sent to the repository administrator: tech-oatao@listes-diff.inp-toulouse.fr

On the key role of the surface of palygorskite nanofibers in the stabilization of hexagonal metastable β - Ag_2CO_3 phase in palygorskite-based nanocomposites

O. Lakbita^{a,b}, B. Rhouta^{a,*}, F. Maury^b, F. Senocq^b, M. Amjoud^a, L. Daoudi^c

^aLaboratoire de Matière Condensée et Nanostructures (LMCN), Faculté des Sciences et Techniques Guéliz, Université Cadi Ayyad, BP 549, Marrakech, Morocco

^bCIRIMAT, Université de Toulouse, CNRS-UPS-INP, ENSIACET, 4 allée Emile Monso, BP 44362, 31030 Toulouse cedex 4, France

^cLaboratoire de Géoscience et Géoenvironnement, Faculté des Sciences et Techniques Guéliz, Université Cadi Ayyad, BP 549, Marrakech, Morocco

ARTICLE INFO

Keywords:

Ag_2CO_3
Palygorskite
M- Ag_2CO_3
 β - Ag_2CO_3
Heterogeneous nucleation
Homogeneous nucleation

ABSTRACT

This study reports an original remarkable effect of fibrous palygorskite clay mineral in the stabilization at the ambient temperature of the metastable hexagonal β -phase of Ag_2CO_3 along with the stable monoclinic one (m- Ag_2CO_3) and the refinement of their particles size (≈ 5 – 10 nm). These structural and microstructural features likely arise owing to heterogeneous nucleation induced by the surface of palygorskite fibers between CO_3^{2-} anions in solution and Ag^+ exchanged palygorskite (Ag^+ -Pal) as reactants kept maturing for short periods, which should not exceed 1 h. Besides, the phase composition of Ag_2CO_3 supported on palygorskite, namely β - and m-structures can be monitored by carrying on appropriate low temperature treatments under CO_2 atmosphere coupled with aging during several months in such a way that either pure β or m single-phases as well as biphased mixtures with controlled composition can be obtained. Taking into account experimental results and literature data, a growth mechanism is discussed.

1. Introduction

Owing to the widespread natural abundance, low cost, safety, layered structure, high surface area, multi-scale porosity, specific properties of cationic exchange characterizing for instance the smectite family and to the presence of significant density of reactive silanol (SiOH) on edges of particles of fibrous clays (e.g. palygorskite, sepiolite) (Bouna et al., 2012; Rhouta et al., 2013), clay minerals more recently have aroused great interest for designing composite materials structured at the nanoscale level (Alcántara et al., 2014; Bouna et al., 2011; Darder et al., 2017; Pérez-Carvajal et al., 2016). In such heterostructures, several kinds of organic (Rahman et al., 2017; Tominaga et al., 2016), bio-organic (Darder et al., 2017; Ilsouk et al., 2017; Roque-Ruiz et al., 2016) and inorganic (Lakbita et al., 2016; Praneeth and Paria, 2017) guest species can be assembled, according to different synthesis approaches based either on intercalation by ion exchange (Roy et al., 2017) or grafting to SiOH groups, with host phyllosilicates (Aït Aghzzaf et al., 2012). These combinations can act in a synergistic way giving rise to multifunctional materials with optimum structural and textural properties which can be destined to various versatile and innovative applications as heterogeneous catalysts in petroleum

cracking (Emam et al., 2008), photocatalysts in environmental protection (Bouna et al., 2011; Lakbita et al., 2016; Pérez-Carvajal et al., 2016), molecular sieves (Liu and Wang, 2017), selective adsorbents (Boudriche et al., 2015; Msaadi et al., 2017), thermal insulators (Darder et al., 2017; Jahani et al., 2015; Laufer et al., 2012), electrochemical, electroanalytical and optical devices (Mudrinić et al., 2015; Tominaga et al., 2016; Kenne Dedzo et al., 2017) and inhibition systems in metallic corrosion (Aït Aghzzaf et al., 2012; Aït Aghzzaf et al., 2014; Aït Aghzzaf et al., 2017).

In this respect, clay minerals of the smectite group (e.g. montmorillonite, beidellite, stevensite) and fibrous ones (palygorskite, sepiolite) were most used for developing mesoporous inorganic heterostructures by supporting SiO_2 , TiO_2 , SiO_2 - TiO_2 , ZnO , Ag_2CO_3 , Ag_3PO_4 functional nanomaterials for environmental and antibacterial applications as degradation of organic pollutants or bacteria by heterogeneous photocatalysis (Aranda et al., 2008; Bouna et al., 2011; Praneeth and Paria, 2017; Roy et al., 2017). These studies were generally focused on physico-chemical characterizations of the composite materials, especially the main features of the grafted nanomaterials in relation with their functional activities. Nevertheless, compared to the abundance of these works quite few were aimed the study of the effect of the clayey support

* Corresponding author.

E-mail address: b.rhouta@uca.ma (B. Rhouta).

on the microstructure and crystallographic structure of the active component.

In this context, one of the studies dealing with this issue is that of TiO₂ supported on palygorskite (Pal) where it was reported that the clay support exerted a beneficial effect by stabilizing remarkably TiO₂ in the metastable anatase form up to very high temperature (900 °C) at which the stable rutile phase is usually obtained (Bouna et al., 2011). Besides, it was found that the supported TiO₂ anatase exhibited very fine-grained particles (≈ 10 nm). This structural feature, which cannot be met with bulk TiO₂, has made these composites exhibit a better photocatalytic activity than commercial TiO₂ powder as Degussa P25 (Bouna et al., 2011).

If TiO₂ is a well-known photocatalyst under UV radiation, Ag₂CO₃ is very attractive for its high activity in the visible range. Many studies dealing with the thermal stability of Ag₂CO₃ in different atmospheres and using different analytical techniques have been published. These include for instance Nagy et al. (1971) by DTA in He and CO₂, Sawada et al. (1989a, 1989b, 1989c, 1991) by DTA in CO₂, Epling et al. (1998) by XPS, ISS and TPR under vacuum, Norby et al. (2002) by synchrotron XRD in CO₂, Atwater (2002) by complex dielectric permittivity and Koga et al. (2013) by TG/DTA in N₂, CO₂ and H₂O vapor, DTA-MS in

He, HT-XRD in N₂ and CO₂ and also by DSC. They have shown that, upon heating under CO₂ atmosphere, the monoclinic phase stable at ambient temperature (P2₁/m, a = 0.4852 nm, b = 0.9549 nm, c = 0.3254 nm, β = 91.97° and Z = 2; JCPDS 01-070-2184) transforms around 150 °C into the intermediate hexagonal β-phase (P31c, a = 0.9172 nm, c = 0.6518 nm and Z = 6; JCPDS 00-031-1236), then at about 210 °C into the high temperature hexagonal α-phase (P-62 m, a = 0.9092 nm, c = 0.3325 nm and Z = 3; JCPDS 00-031-1237) (Norby et al., 2002; Sawada et al., 1989c) before to be, depending on CO₂ pressure, decomposed with CO₂ release beyond 210 °C into Ag₂O and Ag. Then upon cooling from 210 °C to ambient temperature, reverse transformation of α-hexagonal into monoclinic via β-hexagonal was evidenced (Sawada et al., 1989c).

The motivation of this paper is to improve the fundamental understanding of the stabilization of the β-Ag₂CO₃ phase induced by the palygorskite surface, which leads to an original route to synthesize new Ag₂CO₃/Pal photocatalysts exhibiting a high activity under the visible light, as recently demonstrated (Lakbitta et al., 2019). In addition, the phase composition of these nanocomposites can be controlled and the activity of the metastable β-phase was studied while its synthesis is difficult by other methods. Indeed the photocatalytic properties of this metastable phase are not known while those of the stable m-Ag₂CO₃ phase are reported in many papers (Yang and Zhang (2012); Caixia et al., 2014; Xu et al., 2015; Wenjun et al., 2015). At the beginning of this work, we expected different photocatalytic properties in the visible range for both phases since their electronic structure is different. We hoped that the activity of the metastable phase would be greater than that of the stable phase as for TiO₂ anatase (also a metastable phase), which is considered better than rutile (the most thermodynamically stable phase) as photocatalyst under UV light (Carp et al., 2004).

Thus the present paper reports a study on the effects of fibrous palygorskite clay on the stability of the different Ag₂CO₃ phases. Specific thermal treatments under CO₂ coupled to aging for several hours to months were studied on the phase composition (i) of pure Ag₂CO₃ and (ii) of Ag₂CO₃ supported palygorskite composites. This investigation help for establishing correlations between the phase composition of Ag₂CO₃ in Ag₂CO₃/palygorskite new composites and their photocatalytic activity in the visible range which was reported in a companion paper (Lakbitta et al., 2019). The importance of this study is reinforced by the photocatalytic properties since we found that the Ag₂CO₃-Pal nanocomposite in which Ag₂CO₃ was single-phased and crystallized with the stable monoclinic structure was more active than the one crystallizing entirely with the metastable β-Ag₂CO₃ structure. Nevertheless, composite materials containing a mixture of both Ag₂CO₃ phases with a relative content of 32% of β- and 68% of m-phase was

found to be the most efficient photocatalyst of the series. This behavior likely reveals a synergetic effect between both phases in the photocatalytic degradation of Orange G dye under visible light as found for the anatase/rutile TiO₂ couple. This denotes the great interest of developing supported photocatalysts based on clay minerals, which besides present the advantage to flocculate readily making their recovering from treated wastewater easier, without requiring expensive microfiltration.

2. Experimental

2.1. Starting materials

The palygorskite used in this study was isolated from natural clay picked up from Marrakech High Atlas region, Morocco, and exchanged with Na⁺ (labeled Na⁺-Pal) according to respective purification and homoionization procedures described in details elsewhere (Bouna et al., 2011; Rhouta et al., 2013; Aït Aghzzaf et al., 2014). Briefly, an aqueous dispersion of a given mass of raw clay was reacted with hydrochloric solution (1 M) at pH = 4 to remove carbonate impurities. The dispersion was centrifuged, and the solid was washed several times till the supernatant pH almost reached 7. The solid was thereafter treated under stirring during 24 h by NaCl solution (2 M). This operation was repeated twice to assure complete exchange of the charge compensating cations by Na⁺. The treated clay was recovered by repetitive washing with distilled water until chloride-free sample was obtained as confirmed by AgNO₃ test. The fine fraction (particle size < 2 μm) was separated from the 5 wt% dispersion, according to Stokes' law (Holtzapffel, 1985). This operation was repeated several times till the dispersion was almost transparent. The homoionic sodium palygorskite was recovered by centrifugation at 4000 rpm (*i.e.* 1073 × g) for 20 min and dried at 353 K.

Previous characterizations performed by Rhouta et al. (2013) showed that this palygorskite is predominantly dioctahedral, deficient in zeolitic water and associated with 5 wt% of sepiolite. The composition of this palygorskite was found on the basis of 26 oxygen atoms to be (Si_{7.97}Al_{0.03})(Mg_{2.17}Al_{1.46}Fe_{0.40}Ti_{0.05})(Ca_{0.03}Na_{0.07}K_{0.03})O_{20.18}(OH)_{1.94}(H₂O)_{3.88}, 2.43 H₂O. Its CEC (Cation Exchange Capacity), BET specific surface area and total porous volume were assessed to be 21.2 meq·100 g⁻¹, 116 m²·g⁻¹ (in which external surface is around 88 m²·g⁻¹) and 0.458 cm³·g⁻¹ respectively (Rhouta et al., 2013).

The other starting compounds AgNO₃ and Na₂CO₃ were purchased from Aldrich and used as received without further purification.

2.2. Preparation of Pal-Ag₂CO₃ nanocomposites

Several Pal-Ag₂CO₃ composites differing in Ag₂CO₃ content were readily synthesized by a simple wet route. For preparing composites containing X wt% of Ag₂CO₃ (X = 10, 20, 42, 57, 67 and 80 wt%) (labeled Pal-X%Ag₂CO₃; where X wt% is the initial experimental value), 0.5 g of Na⁺-Pal (a constant amount of palygorskite for all syntheses)

Table 1

Molar concentrations of AgNO₃ and Na₂CO₃ aqueous solutions used in the preparation of Pal-X%Ag₂CO₃ composites. The corresponding amount of Ag⁺ involved in these preparations is given in equivalent of CEC of palygorskite.

Pal/X%Ag ₂ CO ₃ X (%)	AgNO ₃ (M)	Na ₂ CO ₃ (M)	Ag ⁺ equiv. CEC (Pal)
10	0.040	0.010	3.3
20	0.090	0.023	8.0
42	0.260	0.065	23.5
57	0.500	0.130	45.5
68	0.770	0.190	70.0
80	1.450	0.360	182.0

was first dispersed under ultrasounds for 15 min in 20 mL of AgNO_3 aqueous solution of a given concentration (Table 1). This dispersion was maintained under stirring for 1 h in the dark. Thereafter, 40 mL of Na_2CO_3 aqueous solution of a given concentration (Table 1) was slowly added dropwise under stirring to the dispersion for 15 min. It is worth noting that the amount of Ag^+ involved in the preparation of Pal- Ag_2CO_3 composites is in excess with respect to CEC of palygorskite as shown in Table 1. The mixture was kept under stirring at ambient temperature and in the dark for either 1 h (protocol 1) or 24 h (protocol 2) of digestion period in the same way than the procedure reported by Nagy et al., 1971. Indeed these authors demonstrated different reactivity of Ag_2CO_3 according to the digestion duration. Accordingly, the derivative compounds were designated as Pal-X% Ag_2CO_3 -1 h and Pal-X% Ag_2CO_3 -24 h respectively. A yellow precipitate, obtained in both conditions of digestion, was recovered by centrifuging at 5000 rpm (*i.e.* 1677 \times g) for 15 min, washed several times with deionized water and thereafter centrifuged twice by using deionized water and once by using ethanol to remove reaction by-products. Finally, the powdered material obtained was dried in an oven at 60 °C for 48 h and stored in the dark for further uses.

Pure Ag_2CO_3 was also synthesized according to the protocol 1 using the same conditions as above but without palygorskite clay mineral.

2.3. Characterizations

X-ray diffraction (XRD) patterns were recorded at room temperature and ambient atmosphere on pure Ag_2CO_3 and Pal- Ag_2CO_3 composite samples in the 2θ range 3–80° with a recording step of 0.02° at a rate of 2 s/step using a Bruker D8–2 diffractometer equipped with a graphite monochromator (Bragg-Brentano configuration; $\text{Cu K}\alpha$ radiation).

The monoclinic-hexagonal phase transformation of Ag_2CO_3 was investigated *in situ* by XRD as a function of the temperature under CO_2 atmosphere. Different samples prepared with and without palygorskite as support material were analyzed in the 2θ range 15–40° using a Bruker D8 Advance diffractometer equipped with a Lynx Eye® detector and a MRI radiation heating chamber (Bragg-Brentano configuration; Ni filtered $\text{Cu K}\alpha$ radiation). The XRD chamber was purged with CO_2 prior the experiment to remove air traces. The measurements were made under a low CO_2 flow rate (50 sccm) to maintain an overpressure slightly higher than one atmosphere. For pure Ag_2CO_3 , the diffractograms were recorded every 25 °C from 50 to 235 °C. An isotherm was maintained at each level for 10 min to record the XRD pattern and then the temperature was increased to the next step using a ramp of 1 $\text{deg}\cdot\text{s}^{-1}$ (Fig. 1a).

In order to investigate if it was possible to control the proportion of each Ag_2CO_3 phases in a composite sample by appropriate heat treatments under CO_2 atmosphere, as well as to study aging of Ag_2CO_3 component, a series of XRD patterns were recorded at room temperature after specific thermal cycles under CO_2 atmosphere. Typically, a composite sample Pal-57% Ag_2CO_3 underwent two heating cycles at 210 °C with an isothermal step at this temperature for 1 h in the first cycle and 5 h in the second one, then a cooling to 50 °C after each heating. The sample was maintained at 50 °C for 12 h before the second heating cycle. Finally, a last XRD pattern was recorded 60 h later after storage under CO_2 atmosphere in the dark at 50 °C. This treatment is schematically shown in Fig. 1b. In an attempt to form pure hexagonal β -phase, the Pal-57% Ag_2CO_3 sample was stored in the dark at the ambient and XRD pattern was recorded after 6 and 7 months of aging. The sample was thereafter, heated and maintained under CO_2 atmosphere for 1 h at 200 °C before performing again XRD analysis. At the end, the sample was cooled down to 50 °C and a last XRD pattern was recorded. This treatment is illustrated by Fig. 1c for 6 months of aging.

A Jeol JSM 6400 scanning electron microscope (SEM) equipped with an Oxford energy dispersive spectrometer, EDS (Si-Li detector; MK program) and a JEOL JEM 2100F transmission electron microscopy (TEM) equipped with a Bruker AXS Quantax EDS analyzer were used

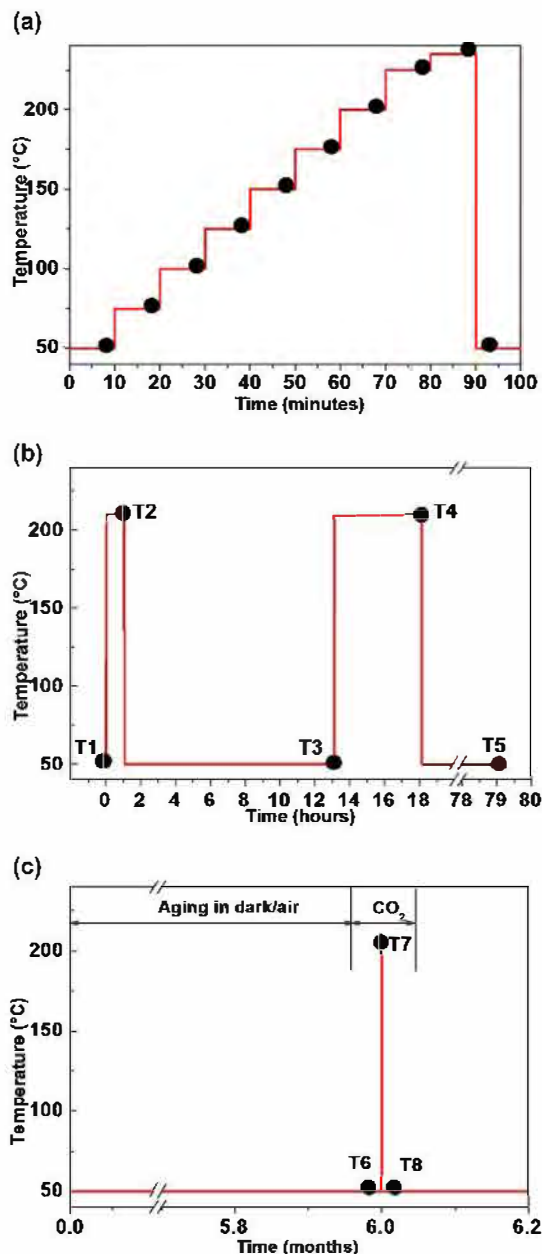


Fig. 1. a) Heating under CO_2 atmosphere ($P \approx 1$ atm) of pure Ag_2CO_3 from 50 to 235 °C at a ramp of 1°/s with isothermal plateau for 10 min every 25 °C (except from 225 to 235 °C) followed by a rapid cooling to the ambient; b) Thermal cycles performed under CO_2 atmosphere on Pal-57% Ag_2CO_3 -1 h sample; c) Heat treatment under CO_2 of Pal-57% Ag_2CO_3 at 200 °C after being aged for 6 months. Dots (●) and T_i ($1 \leq i \leq 8$) indicate temperatures at which *in situ* XRD patterns were recorded.

for characterizing clay particles and performing local elemental analysis.

The mass proportion of each phase in the composite material, *i.e.* β - and m - Ag_2CO_3 and Palygorskite was assessed by XRD from the intensities of representative diffraction peaks of each component. The reflection intensity of (110), (020) and (110) were used respectively for β - and m - Ag_2CO_3 and palygorskite. Practically, the crystallographic structures of the carbonates were modeled by using Carine Crystallography software (Carine software, 1998). Then their XRD diagram was simulated in the interval $6^\circ < 2\theta < 25^\circ$, where there is no annoying overlap, and the comparison with the experimental diagrams allowed to verify that each phase was not textured. Also, XRD patterns of $m + \beta$ mixtures were simulated by varying the proportion of

m- and β -phase in a series of Pal- Ag_2CO_3 composites where the Pal content was set at 0.5 g. The calibration curve given in Fig. S1 (in supplementary information SI-1) was obtained and used to correlate the XRD intensity ratio $(m + \beta)\text{Ag}_2\text{CO}_3/\text{Pal}$ and the corresponding $(m + \beta)\text{Ag}_2\text{CO}_3/\text{Pal}$ mass ratio used in their synthesis. A linear correlation was obtained for $\text{Ag}_2\text{CO}_3/\text{Pal}$ mass ratios lower than 4. After deconvolution of the experimental XRD patterns, the simulated diagrams were fitted by varying the theoretical proportion of each carbonate until a good agreement estimated better than 5%. Examples are given in the supplementary information SI-1.

3. Results

3.1. Structural characterizations

3.1.1. Composition of Pal- Ag_2CO_3 composite

Fig. 2 reports XRD patterns of the starting homoionic compound Na^+ -Pal, two composites synthesized according to protocol 1 (Pal-57% Ag_2CO_3 -1 h) and protocol 2 (Pal-57% Ag_2CO_3 -24 h) and pure Ag_2CO_3 . The sample Na^+ -Pal exhibits a series of characteristic peaks of palygorskite as reported by Rhouta et al. (2013). The characteristic basal reflection (110) of palygorskite is observed at an interplanar distance around 10.56 Å ($2\theta \approx 8.36^\circ$) in good agreement with the JCPDS file 00-021-0958. The absence of carbonates reflections is worth noting and confirms their complete removal in purified Na^+ -Pal while traces of quartz still remain, as evidenced by the detection of the (101) peak at distance around 3.34 Å ($2\theta \approx 26.63^\circ$) (ICDD file N° 03-065-0466) (Rhouta et al., 2013). Almost all the peaks corresponding to palygorskite are also identified in both Pal-57% Ag_2CO_3 samples. This indicates that the fibrous structure of palygorskite remains unaltered in Pal- Ag_2CO_3 composites under the synthesis conditions described above. As expected, pure Ag_2CO_3 sample appears crystallized in the form of the stable monoclinic m-phase as confirmed by the presence of several corresponding intense reflections at the interplanar distances 4.85 Å ($2\theta \approx 18.32^\circ$), 4.78 Å ($2\theta \approx 18.54^\circ$), 4.32 Å ($2\theta \approx 20.50^\circ$), 2.74 Å ($2\theta \approx 32.60^\circ$), 2.66 Å ($2\theta \approx 33.70^\circ$), 2.42 Å ($2\theta \approx 37.07^\circ$) and 2.27 Å ($2\theta \approx 39.60^\circ$) (ICDD file N° 00-026-0339). These peaks are also identified in both Pal-57% Ag_2CO_3 composites denoting the crystallization of m- Ag_2CO_3 in these derivative clayey materials.

Nevertheless, the most striking feature in Pal-57% Ag_2CO_3 composite synthesized according to the protocol 1 is the detection of supplementary reflections at distances around 4.59 Å ($2\theta \approx 19.41^\circ$) and 2.65 Å ($2\theta \approx 33.67^\circ$) which are unambiguously ascribed to the metastable hexagonal β - Ag_2CO_3 structure (ICDD file N°00-031-1236). These peaks are not observed in Pal-57% Ag_2CO_3 -24 h composite elaborated

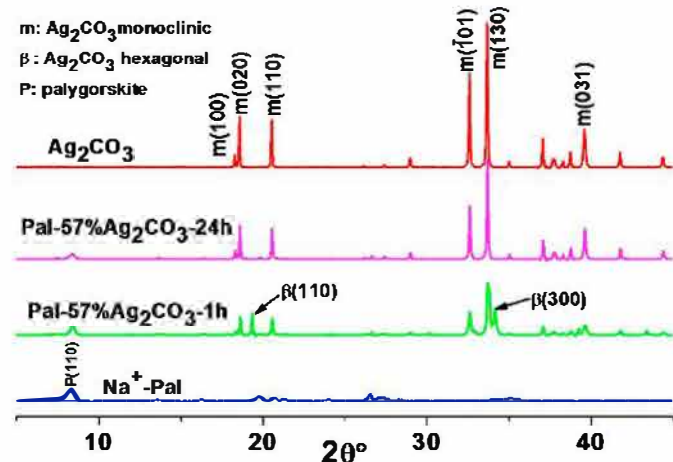


Fig. 2. XRD patterns recorded at room temperature of starting Na^+ homoionized palygorskite (Na^+ -Pal), Pal-57% Ag_2CO_3 -1 h (protocol 1) and Pal-57% Ag_2CO_3 -24 h (protocol 2) nanocomposites, and pure Ag_2CO_3 .

according to protocol 2 denoting that the formation of this metastable phase might not occur in this sample or its amount was lower than the detection threshold of XRD. For instance, traces of Ag_2CO_3 loaded up to 4 wt% in $\text{Ag}_2\text{CO}_3/\text{TiO}_2$ composites were not detected by XRD despite the good crystallinity probably because of the low content and high dispersion (Changlin et al., 2014). On the whole, these results interestingly reveal the coexistence within the composite that underwent a digestion for 1 h (Pal-57% Ag_2CO_3 -1 h) of the two forms of Ag_2CO_3 in addition to palygorskite: the stable monoclinic (m) and metastable hexagonal β -phases. This contrasts with pure Ag_2CO_3 and Pal-57% Ag_2CO_3 -24 h composite obtained upon 24 h of digestion which both exhibit the monophasic m- Ag_2CO_3 structure. These results raise some issues as: is the stabilization of metastable β -hexagonal phase in Pal-57% Ag_2CO_3 -1 h composite promoted by the presence of palygorskite? Does the synthesis protocol play a role in favoring this stabilization? In order to answer these questions, the relative content of each Ag_2CO_3 phases in Pal-57% Ag_2CO_3 -1 h has been analyzed by XRD. Likewise, experiments were undertaken to check the effects of Ag_2CO_3 amount and the digestion duration on the stabilization of the β -phase.

3.1.2. Assessment of m- and β - Ag_2CO_3 content

The relative mass content of each Ag_2CO_3 phase (m and β) in Pal- Ag_2CO_3 composites, whose the total content of Ag_2CO_3 (X) ranged from 10 to 80 wt%, and which were synthesized according to protocol 1 (Pal-X% Ag_2CO_3 -1 h), was assessed from the corresponding most intense XRD reflections for $2\theta < 25^\circ$ and for which no significant overlap exist, i.e. (110) for palygorskite, and (020) and (110) for m- and β - Ag_2CO_3 phases, respectively. The Fig. S1d, supplied as supplementary information (SI-1), shows a good linear variation between XRD intensity ratio $(m + \beta)\text{Ag}_2\text{CO}_3/\text{Pal}$ and the mass ratio $\text{Ag}_2\text{CO}_3/\text{Pal}$ used as starting materials in the synthesis protocol. In all samples of this series, a constant mass of clay set at 0.5 g was used. As a result, this proportional variation has been used as experimental calibration curve to determine the relative content of β - Ag_2CO_3 after deconvolution of experimental patterns.

Fig. 3 shows that the lower total amount of Ag_2CO_3 in Pal- Ag_2CO_3 composite material, the higher fraction of β - Ag_2CO_3 . Beyond a total content of Ag_2CO_3 in the composite of ca. 80 wt%, Ag_2CO_3 crystallizes almost completely with the stable monoclinic structure. Thus, the relative proportion of β - Ag_2CO_3 in the total amount of Ag_2CO_3 formed in the composite tends to increase by decreasing the total Ag_2CO_3 weight

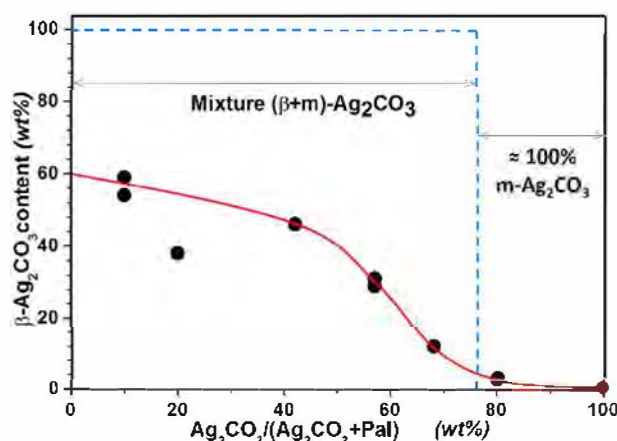


Fig. 3. Relative content of hexagonal β - Ag_2CO_3 in the total amount of Ag_2CO_3 loaded into the composite given by the mass ratio $\beta/(m + \beta)$ as a function of the total mass fraction of Ag_2CO_3 in the composite. The mass of clay was constant at 0.5 g. The solid red curve is a guide for the eyes of the experimental data. The dashed blue lines correspond to the purely heterogeneous model discussed in the text, which separates the β -growth domain from that of the monoclinic phase. (For interpretation of the references to colour in this figure legend, the reader is referred to the web version of this article.)

content, *i.e.* when the relative proportion of palygorskite is more and more dominant in the composite since its content was fixed to 0.5 g. For the lowest Ag_2CO_3 weight contents, the proportion of metastable β -phase tends towards a threshold close to 60%. Consequently, without any treatment, a large proportion of β -phase was able to be stabilized in the composites, which means that this phase is probably stabilized by the surface of palygorskite. Roughly, for composite materials containing a total amount of Ag_2CO_3 lower than *ca.* 80 wt%, the relative fraction of β -phase can be controlled by the total amount of Ag_2CO_3 initially present into as-prepared composite samples. Between *ca.* 50 wt% and 80 wt% of Ag_2CO_3 there is a sharp transition zone. The accurateness and the reproducibility of these assessments is evidenced through their repeatability checked for instance for Pal-10% Ag_2CO_3 and Pal-57% Ag_2CO_3 samples.

3.1.3. Influence of temperature on Ag_2CO_3 structure

3.1.3.1. Pure Ag_2CO_3 . With the attempt to maximize the proportion of metastable hexagonal β - Ag_2CO_3 phase in pure Ag_2CO_3 , *in situ* XRD analyses were achieved as a function of the temperature under CO_2 atmosphere ($P \approx 1$ atm) according to the conditions schematically described in Fig. 1a. The patterns were recorded every 25 °C in the temperature range 50–235 °C and an XRD pattern was also recorded after returning to room temperature (Fig. 4).

In good agreement with the literature (Norby et al., 2002; Sawada et al., 1989a; Sawada et al., 1989b; Sawada et al., 1989c; Sawada et al., 1991; Sawada and Manabe, 1991), it was found that as-prepared pure Ag_2CO_3 exhibits 100% of the monoclinic phase which remains stable till 175 °C as confirmed by the detection of several peaks throughout all the 2θ range explored. At 200 °C, the presence of a shoulder can be noted in the recorded pattern at $2\theta \approx 33.67^\circ$ which could be ascribed to the metastable hexagonal β -structure originating from the transformation of monoclinic phase. This shoulder was observed along with several other intense peaks at 2θ equals to 19.51, 30.00, 33.34 and 34.17° corresponding to the high temperature hexagonal α -phase. The presence of β - Ag_2CO_3 at 175 °C mixed with m - Ag_2CO_3 , confirmed thereafter at 200 °C mixed with α - Ag_2CO_3 denotes that the $m \rightarrow \beta$ phase transition occurs upon heating at an intermediate temperature likely around 180 °C, in good agreement with several authors (Norby et al., 2002; Sawada et al., 1989a; Sawada et al., 1989b; Sawada et al., 1989c; Sawada et al., 1991; Sawada and Manabe, 1991). The β -phase was no longer stable at higher temperature since it is readily transformed at 200 °C into the high temperature hexagonal α -structure. It is worth

noting that upon heating, the reflection (-101) at $2\theta \approx 32.50^\circ$ of the monoclinic phase is shifted towards small angles before vanishing upon its transformation into the β phase. As reported by Masse et al., 1979, this shift could be due to the anisotropic thermal vibration of silver and oxygen atoms within m - Ag_2CO_3 structure. Thereafter, new reflections at 19.54, 32.78 and 37.98° ascribed to Ag_2O (JCPDS 01-072-2108) were observed in the patterns recorded at 225 °C and above. This originates from the decomposition of α - Ag_2CO_3 into the oxide which according to literature, occurs at about 210 °C. Such thermal decomposition has been previously observed either under CO_2 atmosphere at 210 °C (Sawada et al., 1989c) or in air at slightly lower temperature (Sawada et al., 1989a; Sawada et al., 1989b; Sawada et al., 1989c; Sawada et al., 1991; Sawada and Manabe, 1991). Upon cooling to ambient temperature, XRD pattern revealed only the presence of m - Ag_2CO_3 along with an small amount of Ag_2O already formed upon partial decomposition of the carbonate, which confirms the complete reversibility of the transition hexagonal- $\alpha \leftrightarrow$ hexagonal- β and $\beta \leftrightarrow$ monoclinic- m structure (Sawada et al., 1989a; Sawada et al., 1989b; Sawada et al., 1989c; Sawada et al., 1991; Sawada and Manabe, 1991).

3.1.3.2. Pal-57% Ag_2CO_3 composite. As stated above in the section 3.1.1, the composition of Pal- Ag_2CO_3 composite prepared according to protocol 1 has revealed in addition to palygorskite the presence of both m - and β - Ag_2CO_3 in as-prepared materials (T1 in Table 2). Then *in situ* XRD analyses of Pal-57% Ag_2CO_3 -1 h composite were performed under CO_2 atmosphere at 210 °C (T2), at room temperature after 12 h aging under CO_2 (T3), then at 210 °C for 5 h (T4), and finally after aging in the dark for 60 h (T5), according to the treatment conditions schematically described in Fig. 1b and summarized in Table 2. The choice of 210 °C comes from the confirmation by above results it is a critical temperature beyond which the carbonate is decomposed. Fig. 5 shows XRD patterns in the 2θ range 15–25 °C recorded at different steps Ti of this treatment. The reflection at 0.459 nm ($2\theta \approx 19.32^\circ$) corresponding to (110) of the metastable β - Ag_2CO_3 phase along with those at 0.485, 0.478 and 0.432 nm ($2\theta \approx 18.27, 18.55$ and 20.54° respectively) characteristic of m - Ag_2CO_3 were observed in as-prepared nanocomposite. Both phases coexist in addition to palygorskite, in proportions around 18 wt% for β , 39 wt% for m and 43 wt% for Pal (Table 2). Interestingly, all XRD patterns recorded at room temperature showed that the metastable β - Ag_2CO_3 phase is always present by contrast with pure Ag_2CO_3 (Fig. 4). Furthermore the increasing intensity of its XRD peaks by going from the treatment T1 to T4 gives evidence for an increase of its proportion in the composite. Likewise in contrast to pure Ag_2CO_3 , the metastable β - Ag_2CO_3 phase grown in presence of palygorskite did not transform into α - Ag_2CO_3 structure upon heating at 210 °C.

This result demonstrates the remarkable effect of palygorskite in stabilizing the metastable hexagonal β - Ag_2CO_3 phase. A similar effect of stabilization of a metastable phase induced by the surface of palygorskite was recently demonstrated for TiO_2 nanoparticles since the anatase structure was maintained up to 900 °C at the expense of the rutile on the palygorskite fibers (Bouna et al., 2011).

The proportion of β - Ag_2CO_3 in the total amount of Ag_2CO_3 formed into the composite is given by the mass ratio $\beta/(m + \beta)$. It was assessed from (110), (020) and (110) XRD reflection intensities of β -, m - and palygorskite, respectively. The data were taken from Fig. 5 and the results were reported in Table 2. This clearly confirms that the mass fraction of β - Ag_2CO_3 increases after each thermal cycle since starting from 32 wt% it increases to 70 wt% after only two thermal cycles. However after aging in dark for a few days (60 h), the β proportion slightly decreases but stabilizes close to 50% which is larger than the value for as-prepared sample.

Interestingly such a thermal treatment could be an original route to produce 100% of hexagonal β - Ag_2CO_3 supported on palygorskite, which has been investigated hereafter.

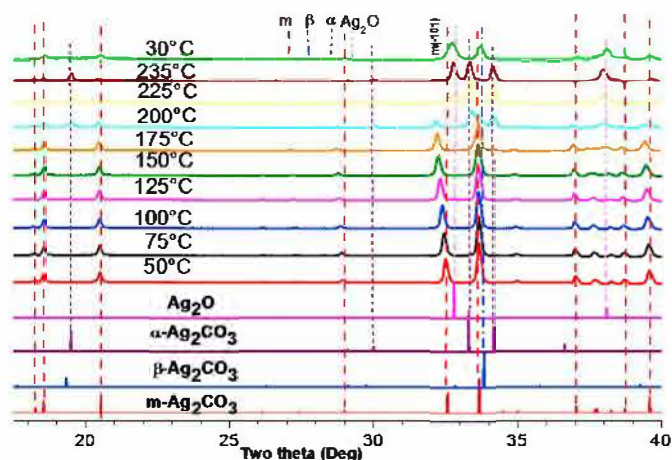


Fig. 4. *In situ* XRD patterns of pure monoclinic Ag_2CO_3 (100% monophased) versus temperature under CO_2 atmosphere ($P \approx 1$ atm) showing upon heating the transformation of stable monoclinic (m) into metastable hexagonal β -phase at 180 °C, then β into hexagonal α -phase at 200 °C. The decomposition of a part of α -phase into Ag_2O occurs at higher temperature. The last pattern shows the reverse transition $\alpha \rightarrow \beta \rightarrow m$ upon cooling to the ambient temperature.

Table 2

Relative content of hexagonal β - Ag_2CO_3 in the total amount of Ag_2CO_3 formed into the composite Pal-57% Ag_2CO_3 -1 h given by the mass ratio $\beta/(m + \beta)$ after the thermal treatment reported in Fig. 1b. The relative contents of each component were assessed from XRD intensities of reflections (110), (020) and (110) of β - and m - Ag_2CO_3 , and palygorskite respectively, and the calibration curve of Fig. S1d.

Treatment number	Conditions of the treatment	$\beta(m + \beta)$ %	β - Ag_2CO_3 (wt%)	m - Ag_2CO_3 (wt%)	Pal (wt%)
T1	As-prepared	32	18	39	43
T2	T1 + 1 h@210 °C under CO_2	50	28.5	28.5	43
T3	T2 + 12 h aging under CO_2	48	27	30	43
T4	T3 + 5 h@210 °C under CO_2	70	40	17	43
T5	T4 + 60 h aging under CO_2	48	27	30	43

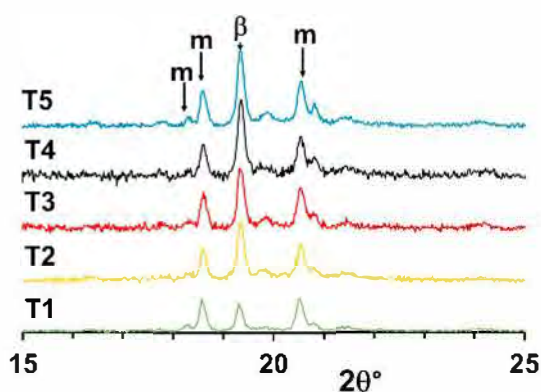


Fig. 5. *In situ* XRD patterns of Pal-57% Ag_2CO_3 -1 h nanocomposite recorded at room temperature under CO_2 atmosphere ($P \approx 1$ atm) immediately after two thermal cycles at 210 °C. The patterns were recorded at temperatures T_i (with $1 \leq i \leq 5$) according to the conditions reported in Fig. 1b.

3.1.4. Influence of aging on Ag_2CO_3 structure

A major result at this stage is the stabilization of β - Ag_2CO_3 probably thanks to the presence of palygorskite leading to as-prepared composite material containing a mixture ($m + \beta$) Ag_2CO_3 . Enrichment of the metastable β -phase was achieved by heat treatments at 210 °C under CO_2 atmosphere to cause the phase transformation $m \rightarrow \beta$.

Other experiments were performed in order (i) to check the reproducibility of above results, (ii) to study the effect of aging on the structural transformation of Ag_2CO_3 and (iii) to determine if it was possible to get 100% of the hexagonal β -structure.

Experiments leading to the results presented in Fig. 5 were repeated using a composite Pal-57% Ag_2CO_3 sample prepared according to protocol 1, in which the initial β - Ag_2CO_3 content was 32% (Table 2). A new series of *in situ* XRD patterns were recorded for two as-prepared samples of the same composition but after 6 and 7 months of aging in the dark and in air. Moreover, As beforehand shown in Fig. 4, because Ag_2CO_3 begins to decompose at $T > 210$ °C to form Ag_2O as by-product (Sawada et al., 1989a; Sawada et al., 1989b; Sawada et al., 1989c; Sawada et al., 1991; Sawada and Manabe, 1991), the temperature treatment was substantially reduced from 210 °C to 200 °C to deviate more from the critical decomposition temperature of this carbonate. The experimental procedure is schematically described in Fig. 1c and the results are shown in Fig. 6 for the sample after 6 months of aging. After the aging period, XRD diagrams were first recorded at the ambient (T6 in Fig. 6), then the samples underwent a rapid temperature increase to 200 °C (1°/s) under CO_2 ($P \approx 1$ atm), and were maintained for 1 h at this temperature where an XRD pattern was recorded (T7). Finally, they were rapidly cooled to room temperature and a last XRD pattern was recorded (T8).

XRD patterns of Pal-57% Ag_2CO_3 -1 h composites after aging for 6 and 7 months are very similar to the one as-prepared (data after 7 months aging are supplied as Fig. S2 in the supplementary information SI-2). In addition to palygorskite, they exhibit a mixture of m - and β - Ag_2CO_3 with a proportion of β -phase of 29% and 30% respectively, which is in the experimental error of the 32% found for as-prepared

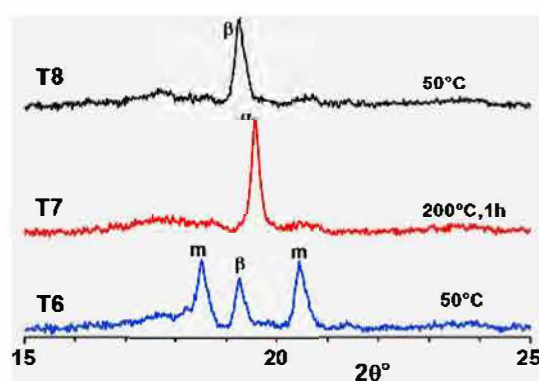


Fig. 6. *In situ* XRD patterns of a Pal-57% Ag_2CO_3 -1 h composite after 6 months aging recorded under CO_2 atmosphere ($P \approx 1$ atm) during a thermal cycle at 200 °C. The patterns were recorded at temperatures T_i (with $6 \leq i \leq 8$) according to the conditions reported in Fig. 1c. The pattern T7 was recorded at 200 °C while both T6 (as-prepared plus after 6 months aging) and T8 (after the cycle at 200 °C) were recorded at 50 °C (near room temperature).

samples before aging (Table 2). Keeping in mind the results found for a fresh composite sample which underwent an almost identical thermal treatment (Fig. 5), the striking result for both aged samples over a long period is that after thermal treatment 100% of Ag_2CO_3 exhibit the hexagonal β -structure, *i.e.* all monoclinic m -phase has been transformed irreversibly (Fig. 6). More precisely, at 200 °C, both m - and β - Ag_2CO_3 phases are completely transformed into another structure already mentioned in the literature as high temperature hexagonal α -phase (Sawada et al., 1989a; Sawada et al., 1989b; Sawada et al., 1989c; Sawada et al., 1991; Sawada and Manabe, 1991). Then, returning to room temperature, the α -phase is completely transformed into β - Ag_2CO_3 . No evidence for the stable monoclinic phase was found for both aged composites upon cooling at the ambient. As a result, by combining a long aging of a few months and this thermal treatment, a synergetic effect produces 100% of hexagonal β - Ag_2CO_3 phase in presence of palygorskite fibers.

In order to check if this structural transformation is induced by the surface of palygorskite or if it could be induced by any surfaces, the same thermal treatment was applied to Ag_2CO_3 supported on Celite. This support is a diatomaceous derivative consisting essentially of porous silica. The sample used was a Celite- Ag_2CO_3 composite material supplied by Aldrich with a silver carbonate content of approximately 50 wt%, *i.e.* very close to the composites based on palygorskite investigated here. Since it was a commercial compound, it was supposed to be aged (*i.e.* not freshly prepared) and, as all silver salts, it was supplied and stored in a dark glass bottle, *i.e.* in conditions that are not so different. The same thermal treatment described in Fig. 1c was applied to a Celite- Ag_2CO_3 composite sample and the result is reported in Fig. 7.

In as-received Celite- Ag_2CO_3 composite sample, Ag_2CO_3 was found 100% monoclinic (T6 in Fig. 7). No evidence for the metastable hexagonal phases was found by contrast with Pal- Ag_2CO_3 composite. At 200 °C no significant change occurs in the XRD pattern (T7) except a

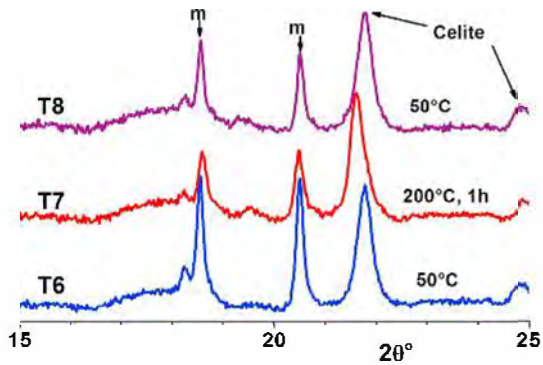


Fig. 7. *In situ* XRD patterns of a Celite- Ag_2CO_3 composite sample recorded under CO_2 atmosphere ($P \approx 1$ atm) during a thermal cycle at 200°C . The patterns were recorded at temperatures T_i ($6 \leq i \leq 8$) according to the conditions reported in Fig. 1c. The pattern T7 was recorded at 200°C while both T6 (as-received) and T8 (after the cycle at 200°C) were recorded at 50°C (near room temperature).

slight increase of the Celite peak at about 21.8° which likely results from a better crystallinity induced by annealing. A small shift of this peak towards low angles was also observed due to the thermal expansion of the structure. After returning to 50°C , XRD pattern (T8) is the same than the previous ones. No phase transformation of silver carbonate was observed, which indicate this silica-related support is inert. This confirms that the surface of palygorskite plays a major role in the stabilization of the metastable $\beta\text{-Ag}_2\text{CO}_3$ phase.

3.2. Microstructural characterizations

Palygorskite is a clay material made up of fibers of several micrometers long and tens of nanometers wide as shown by the Fig. 8a. At low magnification, SEM analysis of Pal-57% Ag_2CO_3 -1 h composite shows that Ag_2CO_3 particles are fixed on and retained into the tangle of palygorskite fibers (Fig. 8b). The Ag_2CO_3 particles exhibit relatively large size distribution from a few tens of nm to almost $1\ \mu\text{m}$. By contrast, those grown in the same conditions in bare Ag_2CO_3 , i.e. without palygorskite, exhibit micrometric size (Fig. 8c). Considering the nanometric width of palygorskite fibers on one hand, and the relatively large size dispersion of Ag_2CO_3 particles starting at the nanometric scale, the sample Pal-57% Ag_2CO_3 -1 h representative of the series can be considered as a nanocomposite material.

TEM analyses were performed to complete the above SEM results and try to directly observe the different phases. Fig. 9a shows a micrograph of as-prepared Pal-57% Ag_2CO_3 -1 h nanocomposite. Mainly due to the handling of the sample, which modified the phase dispersion

in the powdered composite, it exhibits heterogeneous zones with uncoated, partially coated and continuously coated palygorskite fibers. Also, Ag_2CO_3 is found on one hand as agglomerated nanoparticles (NPs) forming micrometric porous particles trapped into the fibers entanglement, and on the other hand, as individual NPs attached and likely directly grown on the surface of palygorskite fibers (Fig. 9b). NPs fixed on fibers are sparse and monodisperse with an average size of approximately 10 ± 2 nm. In the zone of Fig. 2b, Palygorskite fibers are only partially covered by Ag_2CO_3 NPs leading to a low coverage and a low surface density. In this case, no merge or coalescence of NPs is observed; NPs do not touch each other and do not form aggregates or continuous coating (Fig. 9b). In addition to the handling of the sample, which is a factor accentuating the heterogeneity of a sample, another reason explaining why some fiber surfaces were not uniformly coated would be because they were not accessible for the growth of Ag_2CO_3 during the synthesis.

Selected area electron diffractions of both agglomerated Ag_2CO_3 NPs and sparse Ag_2CO_3 NPs grown on palygorskite have revealed at least three rings at interplanar distances of about 4.68, 2.69 and 2.26 Å which are unambiguously indexed to (020), (-130) or (-101) and (031) reflections respectively of $m\text{-Ag}_2\text{CO}_3$ (Fig. 9c). No evidence for the hexagonal β -phase was found by TEM diffraction even for individual NP attached on the palygorskite surface.

Interestingly, in parts of the sample, some palygorskite fibers are completely and uniformly coated by Ag_2CO_3 NPs. With an average size of ca. 20 nm the NPs form a continuous and compact monolayer with a good conformal coverage of the fibers whose mean diameter was ca. 80 nm, as shown in Fig. 9d. In this area, there is no evidence for the growth of a 2nd and a 3rd monolayer of Ag_2CO_3 NPs on the top of the 1st one. The Table inserted in Fig. 9 gives the EDS analysis of the conformal coating shown in Fig. 9d. The experimental Ag/C atomic ratio (1.94) is in very good agreement with the theoretical value for Ag_2CO_3 (2.0). Also, the other atomic ratios, which are representative of the palygorskite are very coherent with the values expected for this clay mineral, as reported in section 2.1. This confirms the presence of a Pal fiber inside the conformal coating that forms a sheath and reveals that the compact monolayer of Ag_2CO_3 NPs has grown directly on the surface of Pal fiber in this zone of the sample.

In other areas of samples analyzed by TEM, submicron and even micron aggregates are entangled in bare fibers, as shown in Fig. 10. The Table inserted in this Fig. 10 gives point EDS analyses compared to the values expected for Ag_2CO_3 and palygorskite. With an atomic ratio Ag/C of 1.7, the analysis of an aggregate (position #2) confirms it is composed of Ag_2CO_3 NPs (theoretical value 2.0). Also, the other atomic ratios analyzed at this location #2 reveal the presence of palygorskite fibers within this aggregate. It is therefore possible that at this location, several monolayers of NPs have grown on a first monolayer of Ag_2CO_3 NPs and are stacked up to form this 3D particle. This growth mode

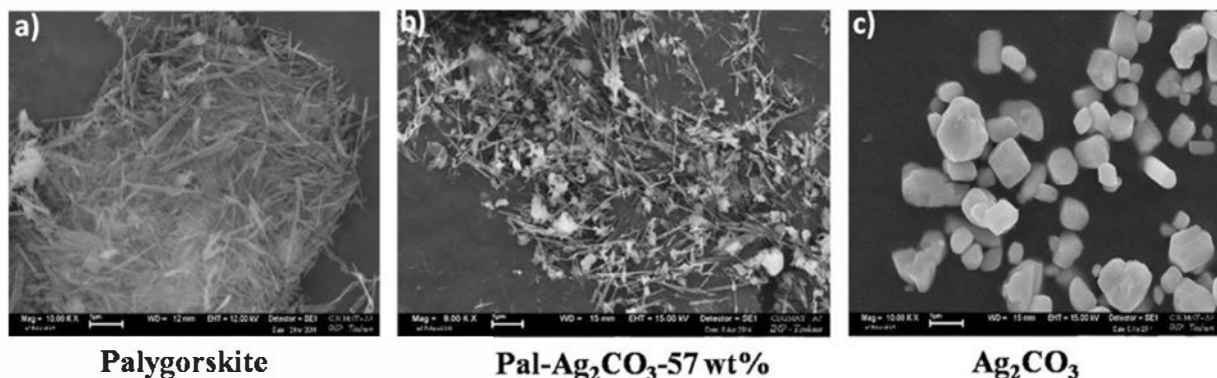


Fig. 8. SEM micrographs showing (a) pristine palygorskite fibers, (b) very fine Ag_2CO_3 particles immobilized onto and into palygorskite fibers (Pal-57% Ag_2CO_3 -1 h) and (c) polyhedral and well faceted Ag_2CO_3 crystals. The samples shown in micrographs (b) et (c) were prepared in the same conditions in terms of AgNO_3 and Na_2CO_3 initial concentrations as indicated in the experimental section.

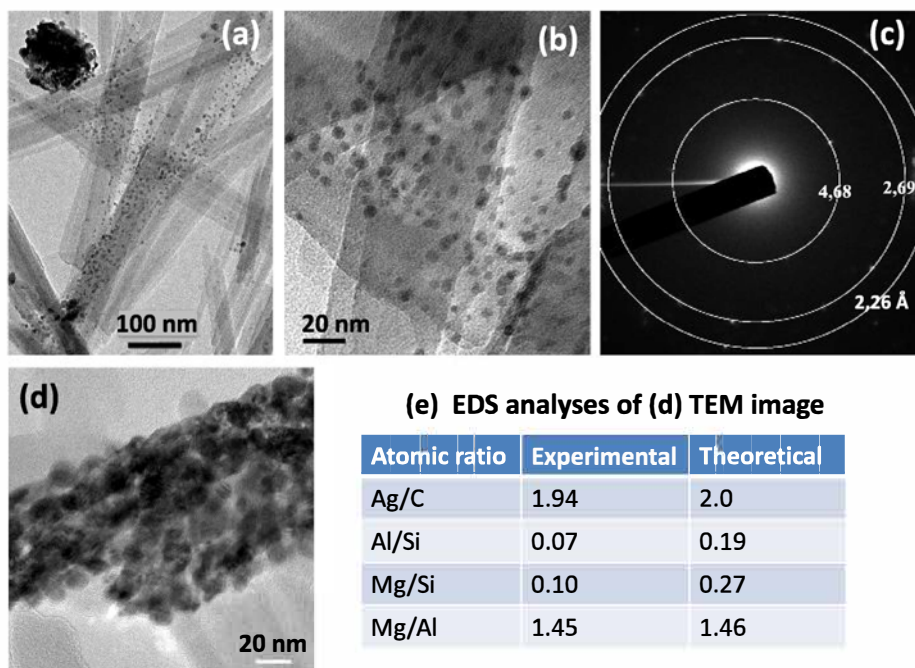


Fig. 9. TEM analysis of a composite sample Pal-57%Ag₂CO₃: (a) low and (b) high magnification micrographs showing heterogeneities with both a sparse growth of Ag₂CO₃ NPs on the surface of palygorskite fibers and submicron agglomerated NPs; (c) selected area diffraction pattern of image (b) showing that all the diffraction spots are on the rings corresponding to m-Ag₂CO₃; (d) conformal coverage of a Pal fiber by a continuous and compact monolayer of Ag₂CO₃ NPs; (e) EDS analysis of TEM image (d).

contrasts with the continuous conformal coverage of a monolayer shown in Fig. 9d. The bare fiber EDS analysis (position #1) is in good agreement with the expected values (except for an excess of Mg at this location). However it is remarkable that traces of Ag are found (0.4 at %). The origin of silver could be an ion exchange as discussed later.

4. Discussion

4.1. Influence of palygorskite on phase formation of Ag₂CO₃

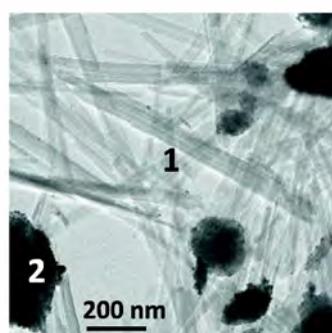
In good agreement with the literature (Norby et al., 2002; Sawada et al., 1989a; Sawada et al., 1989b; Sawada et al., 1989c; Sawada et al., 1991; Sawada and Manabe, 1991), pure Ag₂CO₃ was found to crystallize at the ambient in the form of stable monoclinic structure (Figs. 2 and 4) with micrometric crystal sizes (Fig. 7c). Upon heating, monoclinic XRD peaks, especially (-101), progressively shift towards small angles before vanishing and giving rise to the intermediate hexagonal β -structure at around 180 °C as reported by the literature (Norby et al., 2002; Sawada et al., 1989a; Sawada et al., 1989b; Sawada et al., 1989c; Sawada et al., 1991; Sawada and Manabe, 1991) (Fig. 4). Increasing further the temperature, the β -phase is transformed into hexagonal α -phase which in turn undergoes a partial decomposition into Ag₂O starting around 210 °C. Before thermal decomposition the phase transformations of Ag₂CO₃ were reversible.

Such a behavior was not observed in presence of palygorskite. Indeed, it is worth noting that β -Ag₂CO₃ was retained at the ambient along with the stable monoclinic phase in Pal-X%Ag₂CO₃ composites, when they were synthesized according to protocol 1, *i.e.* when the reagents Pal, AgNO₃ and Na₂CO₃ underwent a digestion for 1 h. In this respect, Ag₂CO₃ particles appear nanometric in size, many of them are agglomerated and trapped in the tangle of palygorskite fibers (Fig. 8b), others are immobilized and scattered on the fiber surfaces of clay mineral (Fig. 9). These salient results give evidence for the key role of palygorskite in the refinement of Ag₂CO₃ particles and in the stabilization of the metastable hexagonal β -phase.

4.2. Influence of palygorskite on nucleation mechanism of Ag₂CO₃

The differences in average particle size and in crystallographic structure of Ag₂CO₃ when it is synthesized without or with palygorskite as support material could be due to different nucleation mechanisms since heterogenous nucleation can play a key role in presence of palygorskite nanofibers.

In the synthesis of pure Ag₂CO₃, *i.e.* without palygorskite, the nucleation and growth occur obviously in homogeneous aqueous solutions. As a result, Ag₂CO₃ crystallites can grow to form small crystals with regular shape and size. Their growth is not limited by the nucleation rate. The size distribution is relatively narrow and they reach a

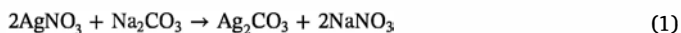


Point EDS analyses

Atomic ratio	Experimental # 1	Exp. # 2	Theoretical
Ag/C	(0.39 at% Ag)*	1.66	2.00
Al/Si	0.05	0.24	0.19
Mg/Si	0.31	0.27	0.27
Mg/Al	5.99	1.11	1.46
Fe/Si	0.04	nd	0.05

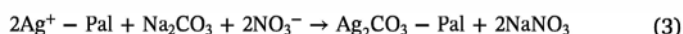
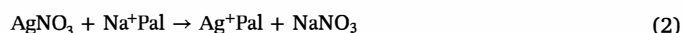
Fig. 10. TEM analysis of another composite Pal-57%Ag₂CO₃ sample showing the presence of submicron agglomerated Ag₂CO₃ NPs and bare palygorskite fibers. The table gives experimental EDS analyses at the locations indicated on the TEM image.

micrometric average size. These particles are well faceted and exhibit polyhedral shape and short rod-like morphologies (Fig. 8c). This is in agreement with previous works (Xu et al., 2015). Under this synthesis condition, the density of nucleation sites is low and the critical radius required for nuclei stabilization is relatively large since there are no spatial constraints. Consequently, the growth of the stable monoclinic phase occurs readily without evidence for other structures as demonstrated by XRD (Fig. 2). The reaction mechanism based on such homogeneous nucleation would correspond to Reaction (1):



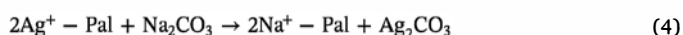
In the synthesis of Pal- Ag_2CO_3 composites, the growth of Ag_2CO_3 may also occur according to Reaction 1, i.e. via homogeneous nucleation. However the palygorskite fibers can have two important effects. First, they can act as inert solid that, under vigorous stirring conditions of the aqueous dispersion, will increase homogeneous nucleation rate. This will induce a higher nucleation density and consequently a higher number of Ag_2CO_3 crystallites with a reduced average size. Also, flux heterogeneities induced by agitation can generate concentration gradients in the solution (vortices...) that will result in the agglomeration of particles. This growth mode may lead to a large size distribution and to particles agglomerated and trapped in the tangle of palygorskite fibers as observed in Fig. 9a and Fig. 10. These particles will not be strongly attached to the surface of palygorskite since no interfacial reaction is involved in the growth mechanism. As second route, palygorskite may also act as support material that will induce heterogeneous nucleation. Here it is necessary to remember that the palygorskite used was beforehand exchanged with Na^+ ions according to homoionization procedure previously reported (Rhouta et al., 2013). This so formed Na^+ -Pal was carbonate-free as evidenced by XRD (Fig. 2) and was first sonically dispersed in AgNO_3 aqueous solution for 15 min and stirred for 60 min before introducing Na_2CO_3 into the dispersion. During this period where there is no carbonate in the solution, AgNO_3 may start to react by ion exchange with Na^+ ions of palygorskite on the surface of the fibers to form Ag^+ exchanged palygorskite (Ag^+ -Pal) according to the Reaction (2). This will greatly facilitate further heterogeneous nucleation on adsorbed Ag^+ ions and the growth of Ag_2CO_3 directly onto the functionalized surface of palygorskite with a relatively strong interface. This heterogeneous growth

mode can be represented by both the Reactions (2) and (3) and it is also schematized in Fig. 11.



As a result, the Ag_2CO_3 particles formed by this heterogeneous growth mode must be strongly attached to the palygorskite fibers and their average size should be very small due to high nucleation density induced by surface defects or steric effects (Fig. 9).

The stability of Ag^+ -Pal in presence of Na_2CO_3 could to be enhanced by short digestion durations (≤ 1 h; protocol 1) to allow the growth of Ag_2CO_3 onto palygorskite fibers (Reaction 3). For higher digestion times, e.g. 24 h (protocol 2), the same mechanism must occur in the early stages, but a kinetically competing mechanism may occur for longer digestion time. Thus as far as the digestion period increased, a given proportion of supported β - Ag_2CO_3 could be dissolved releasing Ag^+ ions in the aqueous solution according to Reaction (4):



This dissolution hypothesis is supported by the following data. The CEC of palygorskite involved herein is low, about 21.2 meq/100 g (Rhouta et al., 2013). Thus, no > 0.11 mmol of Ag^+ can be adsorbed on 0.5 g of palygorskite yielding therefore 0.11 mmol of supported β - Ag_2CO_3 , i.e. 30 mg of β - Ag_2CO_3 . Although poorly soluble in water (Seidell and Linke, 1919), the solubility of Ag_2CO_3 at 20 °C is 32 mg/L, and by taking into account the volume of aqueous solution involved in this study (60 mL total corresponding to a mixture of 20 mL for AgNO_3 and 40 mL for Na_2CO_3), at least 1.92 mg of β - Ag_2CO_3 or in other words ca. 7% of the β - Ag_2CO_3 formed in the early stage could be dissolved during long incubation times. This is not negligible. Furthermore such a dissolution could be further favored on one hand by kinetic considerations due to long digestion time and on the other hand by structural and microstructural characteristics of solid particles (Gout et al., 1974). Thus, this dissolution could be favored both by the hexagonal structure of the metastable β -phase and the nanometric average size of these supported β -particles. Hence, the dissolution of certain proportion of β - Ag_2CO_3 would result in the reverse exchange Reaction (4) restoring Na^+ -Pal and yielding the formation of Ag_2CO_3 by

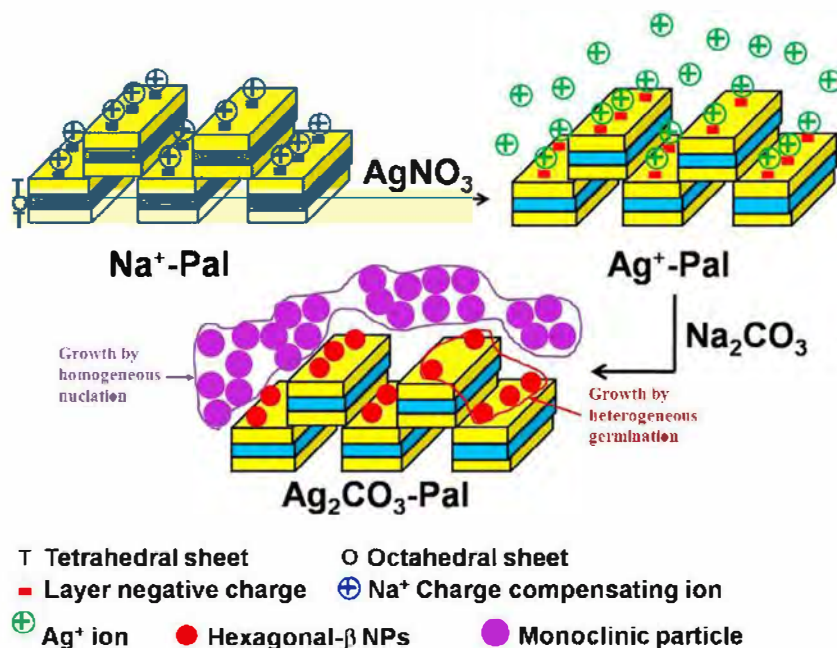


Fig. 11. Schematic illustration of heterogenous growth of hexagonal β -NPs on the surface of palygorskite fibers and of monoclinic m- Ag_2CO_3 particles by a competitive homogeneous route.

homogeneous reaction between Ag^+ ions released from palygorskite surface and carbonates in solution. As a result, in the chemical mechanism of composite synthesis involving long duration times, Ag_2CO_3 is likely formed mainly according to homogeneous nucleation (Reaction 1), which leads as in the case of pure Ag_2CO_3 to a structure 100% m- Ag_2CO_3 , as supported by Fig. 2.

The fact that Ag_2CO_3 crystallizes with two different structures (α and β) in the composite material synthesized with a short digestion period supports the idea that they could originate from the two mechanisms above mentioned. This suggests that each mechanism leads to one phase and both are possible at once. The stable phase m- Ag_2CO_3 would be grown mainly by homogeneous nucleation (Reaction 1), while there is strong evidence that the metastable β - Ag_2CO_3 phase would result from heterogeneous growth mode (Reactions 2 and 3). It has been previously demonstrated that heterogeneous nucleation on palygorskite surface promoted the growth of the metastable phase TiO_2 anatase at the expense of rutile (Bouna et al., 2011). We also think it is a good hypothesis to propose that β - Ag_2CO_3 NPs are formed, stabilized and strongly attached to palygorskite nanofibers, and that they grow to form a compact and conformal coating as in Fig. 9d.

Besides, one can admit that the two routes leading to Ag_2CO_3 formation, i.e. on Pal fiber surfaces and in aqueous solution, are two conditions where local concentrations are different. The adsorption of reactive Ag^+ ions on the surface of Pal fibers, upon their exchange with Na^+ ions, would provide a relatively high local concentration of reagents close to the surface favorable to the growth of β - Ag_2CO_3 . In contrast, unattached Ag^+ ions in a dilute aqueous solution relatively far from the surface of Pal fibers could react with CO_3^{2-} ions and produce m- Ag_2CO_3 . This hypothesis allows to consider (i) β - Ag_2CO_3 formed in concentrated-like medium as “inactive” phase, i.e. as non-transformable phase, and (ii) m- Ag_2CO_3 formed in diluted-like medium as “active” phase, i.e. which can be transformed by heating treatments using the name and approach reported by Nagy et al. (1971).

On the other hand, it was confirmed that when Ag_2CO_3 particles were not supported on palygorskite fibers, they agglomerate to an average size of up to 60 μm , which is bigger than those immobilized on the palygorskite surface. This again supports the key role of palygorskite fibers in decreasing Ag_2CO_3 particles size by acting as heterogeneous nucleation sites.

Nevertheless, in contrast to XRD results, TEM analysis did not reveal directly the presence of hexagonal β - Ag_2CO_3 in as-prepared Pal-57% Ag_2CO_3 -1 h sample. There are at least two main reasons. First, unlike XRD, TEM is a local analysis that makes difficult to observe small amounts of a component in a composite material since the proportions are: 18 wt% hexagonal, 39 wt% monoclinic and 43 wt% palygorskite (Table 2). Secondly, and likely the most important reason could be its instability under the electronic beam into the high vacuum of the microscope. This issue would require further TEM investigations but metastable phases are frequently difficult to observe by TEM due to their instability towards the electronic impact, which is more energetic than an X-ray beam. For instance, a metastable metallic δ -Cr phase, thermally stable up to about 400 $^\circ\text{C}$, were identified by different techniques including XRD but was not observed directly by TEM using the same microscope and under similar conditions of this work (200 kV as beam energy) due to *in situ* phase transformation (Michau et al., 2017). This was also the case for the AgBr phase loaded on palygorskite (Yang and Zhang, 2012).

4.3. β - Ag_2CO_3 vs. load in the composite: Heterogeneous growth model

In this section, a simple geometric model is proposed to discuss correlation between the conformal coating of Pal fibers grown by the heterogeneous mechanism and the relative content of β - Ag_2CO_3 . First, it is assumed that Ag_2CO_3 NPs exhibit monodisperse spherical shape with an average diameter $d = 10$ nm, as supported by TEM characterizations (Fig. 9b). In order to produce a continuous monolayer of NPs

on the surface of Pal fibers the distribution of such NPs might be organized in a compact 2D network. This would be in agreement with Fig. 9d. A good hypothesis for such 2D network is to consider diamond cells, as schematized in Fig. S3. In this structure, as developed in the Supplementary Information SI-3, the planar packing factor corresponding to the ratio between the real surface occupied by a single Ag_2CO_3 NP occupying the diamond cell and the diamond surface is 91%, which means that a maximum of 91% of the Pal surface can be occupied by Ag_2CO_3 NPs. Knowing that the specific external surface area ($S_{\text{ext-Pal}}$) of this palygorskite determined by Rhouta et al. (2013) is ca. 88 m^2/g , the effective fiber surface (S_{eff}) that can be covered with Ag_2CO_3 NPs can be determined as a function of the load of palygorskite in the composite (m_{Pal}) fixed at 0.5 g for the sample series of Fig. 3. Other details on the development of this heterogeneous model are reported in the Supplementary Information (SI-3). At the end, the total mass of deposited Ag_2CO_3 NPs ($m_{\text{Ag}_2\text{CO}_3}$) can be calculated knowing Ag_2CO_3 density ($\rho_{\text{Ag}_2\text{CO}_3}$), the volume of a spherical NP (V_{NP}), the specific external surface area ($S_{\text{ext-Pal}}$), the load of Pal in the composite (m_{Pal}) and the surface area of a spherical NP projected on a plane (S_{NP}) according to the relation:

$$m_{\text{Ag}_2\text{CO}_3} = (\pi^* \rho_{\text{Ag}_2\text{CO}_3} * V_{\text{NP}} * S_{\text{ext-Pal}} * m_{\text{Pal}}) / (S_{\text{NP}} * 2\sqrt{3}) \quad (\text{R1})$$

From Relation R1, the total mass of Ag_2CO_3 NPs that can be immobilized on Pal fibers is 1.604 g for a load of 0.5 g of Pal in the composite, which corresponds to a maximum mass fraction of Ag_2CO_3 for an entire coverage of Pal fibers of ca. 76 wt%. Taking into account our hypothesis stating that β - Ag_2CO_3 grown on the surface of Pal fibers while m- Ag_2CO_3 is formed in the homogeneous phase, this threshold of total Ag_2CO_3 content in the composite of ca. 76 wt% would correspond to the highest total content of Ag_2CO_3 in the composite beyond which additional Ag_2CO_3 can be formed only with the monoclinic structure.

Interestingly, experimental values of Fig. 3 show a sharp change at ca. 76 wt% of total Ag_2CO_3 content, which is also the threshold value above which Pal fibers would be completely coated as predicted by the simple heterogeneous model (blue dashed straight lines in Fig. 3). The β -phase proportion tends to be negligible above this threshold. Experimentally it is likely present but more and more difficult to quantify compared to m- Ag_2CO_3 , as written in section 3.1.1. For total Ag_2CO_3 content below this critical threshold, the discrepancy with the heterogeneous model can be explained by the assumptions of the model that are not sufficiently satisfied. For example, (i) the irregularity of shape and average size decreases the planar packing factor, (ii) a 2nd and even more monolayers of Ag_2CO_3 NPs can grow on the top of the 1st one before it is continuous and complete leading to 3D growth as observed in Fig. 10, (iii) the access to parts of Pal surface can be partially prevented...

Also, the fact that the experimental relative content of β -phase tends to stabilize at about 60% (instead of the theoretical value of 100%) for low Ag_2CO_3 total content in the composite (Fig. 3) could be due to limitation imposed by CEC of palygorskite. Indeed, taking into account the CEC of about 21.2 meq/100 g of the palygorskite investigated elsewhere (Rhouta et al., 2013), the amount of exchanged Ag^+ corresponding to the equivalent of 1 CEC could not exceed 0.11 meq for 0.5 g of Na⁺-Pal used herein. As described in experimental section (2.2), the amount of Ag^+ involved in the synthesis of Pal-10% Ag_2CO_3 is 3.5 times the CEC of palygorskite. Thus, no > 0.11 mmol of Ag^+ can be adsorbed on 0.5 g of palygorskite and could allow the formation of β -phase while Ag^+ excess would be contained in the solution where it could contribute to the formation of m- Ag_2CO_3 as stated above.

4.4. Effect of thermal treatment

The relative content of β - Ag_2CO_3 in the composite could be further increased by performing thermal cycles under CO_2 atmosphere. Indeed, as evidenced from findings gathered in Table 2, after the 1st cycle the

proportion of hexagonal β - Ag_2CO_3 increases from 32% to 50%, then it is stable for 5 h in the dark and again it increases to 70% after the 2nd cycle. So, each thermal cycle acts as a non-return pawl to stabilize the metastable phase. This is likely due to the transformation of m- to β -phase at each step. Upon cooling to room temperature a significant amount of β -phase is not reversibly transformed into the monoclinic structure (by contrast with pure Ag_2CO_3 without palygorskite) probably because of its stabilization by direct interactions with the surfaces of both palygorskite and β -phase already formed. For the sample with a high content of β -phase (70%), possibly a small fraction of this metastable β -phase is not directly in contact with the palygorskite, for instance it could be in the form of small agglomerates resulting from 3D growth on palygorskite like particles agglomerated around fibers in Fig. 10. As a result, this metastable phase would be slowly transformed into the stable monoclinic phase during aging at the ambient for 60 h in the dark.

The coupling between aging for several months and thermal cycles produced synergetic effects that increase significantly the proportion of β - Ag_2CO_3 until it reaches 100%. Possibly aging for several months allows m- Ag_2CO_3 particles to form discontinuous layers or agglomerates on β - Ag_2CO_3 NPs grown on palygorskite fibers. Moreover, the proportion of m- Ag_2CO_3 in aged samples was pretty the same than that in fresh sample. Then, upon heating under CO_2 atmosphere at 200 °C, these m- Ag_2CO_3 particles could be transformed into β -structure that would remain stable upon cooling at the ambient because in turn they would be supported and stabilized for instance by epitaxy on underlying β -particles which have grown directly on palygorskite surface.

5. Conclusions

This study reports the immobilization of Ag_2CO_3 NPs on fibers of natural palygorskite by a simple and easy wet route to produce a new and efficient photocatalyst. The palygorskite significantly decreases the average size of Ag_2CO_3 particles leading to a nanocomposite material with a monodisperse distribution of Ag_2CO_3 NPs known to be an active photocatalyst in the visible light.

The most salient result is the ability of the palygorskite surface to stabilize the metastable β -phase of Ag_2CO_3 . This hexagonal phase likely originates from a heterogeneous mechanism controlled by nucleation rate, which occurs onto the surface of palygorskite nanofibers. This growth mode would compete with a homogenous nucleation taking place in aqueous solution and both growth mechanisms would occur simultaneously. This leads to metastable β - Ag_2CO_3 NPs immobilized onto the fiber surface and to stable m- Ag_2CO_3 submicrometric particles, which tend to form agglomerates trapped in tangled fibers.

It was demonstrated that the proportion of β - Ag_2CO_3 in the nanocomposite can be increased by specific post-treatments. Thus, original thermal cycling under CO_2 atmosphere (inspired from the literature) coupled to aging for several months produces a synergetic effect that allows reaching 100% of β - Ag_2CO_3 in the composite material. Therefore this study sets up different experimental protocols to synthesize new Ag_2CO_3 -Pal nanocomposites for which the crystallographic structure of the functional component Ag_2CO_3 can be controlled from 100% stable monoclinic (m) to 100% metastable hexagonal β through an adjusted mixture of m- and β - Ag_2CO_3 in presence of palygorskite.

Subsequently the photocatalytic activity of these three categories of Ag_2CO_3 /Pal nanocomposites with various phase compositions has been studied under visible light irradiation. Details reported in a companion paper (Lakbita et al., 2019) that the nanocomposite in which Ag_2CO_3 was single-phased with the hexagonal structure was less active than the one crystallizing entirely with the stable monoclinic structure. However, the nanocomposite material containing a mixture of both Ag_2CO_3 phases with a relative content of 32% of β - and 68% of m-phase was found to be the most photoactive material of the series. This behavior revealed a synergetic effect between both Ag_2CO_3 phases in the photocatalytic degradation under visible light of the Orange G dye selected

as model pollutant.

Acknowledgement

The financial supports from the “Programme d'Action Intégrée Volubilis” (N 14/SM/14) and the Project of PPR-CNRST “Domaines Prioritaires de la Recherche Scientifique et du Développement Technologique” (PPR1/2015/63) are gratefully acknowledged.

Appendix A. Supplementary data

Supplementary data to this article can be found online at <https://doi.org/10.1016/j.clay.2019.02.023>.

References

- Ait Aghzzaf, A., Rhouta, B., Steinmetz, J., Rocca, E., Aranda, L., Khalil, A., Yvon, J., Daoudi, L., 2012. Corrosion inhibitors based on chitosan-heptanoate modified beidellite. *Appl. Clay Sci.* 65–66, 173–178. <https://doi.org/10.1016/j.clay.2012.04.025>.
- Ait Aghzzaf, A., Rhouta, B., Rocca, E., Khalil, A., Steinmetz, J., Ait Aghzzaf, A., Rhouta, B., Rocca, E., Khalil, A., Steinmetz, J., 2014. Corrosion inhibition of zinc by calcium exchanged beidellite clay mineral: a new smart corrosion inhibitor. *Corros. Sci.* 80, 46–52. <https://doi.org/10.1016/j.corsci.2013.10.037>.
- Ait Aghzzaf, A., Rhouta, B., Rocca, E., Khalil, A., 2017. Grafted palygorskite as containers of heptanoate for corrosion protection of steel in NaCl medium. *Corros. Sci.* 114, 88–95. <https://doi.org/10.1016/j.corsci.2016.10.028>.
- Alcántara, A.C.S., Darder, M., Aranda, P., Ruiz-Hitzky, E., 2014. Polysaccharide-fibrous clay bionanocomposites. *Appl. Clay Sci.* 96, 2–8. <https://doi.org/10.1016/j.clay.2014.02.018>.
- Aranda, P., Kun, R., Martín-Luengo, M.A., Letaief, S., Dékány, I., Ruiz-Hitzky, E., 2008. Titania–Sepiolite nanocomposites prepared by a surfactant templating colloidal route. *Chem. Mater.* 20, 84–91. <https://doi.org/10.1021/cm702251f>.
- Atwater, J.E., 2002. Complex dielectric permittivities of the $\text{Ag}_2\text{O-Ag}_2\text{CO}_3$ system at microwave frequencies and temperatures between 22 °C and 189 °C. *Appl. Phys. A Mater. Sci. Process.* 75, 555–558. <https://doi.org/10.1007/s003390201308>.
- Boudriche, L., Calvet, R., Chamayou, A., Hamdi, B., Balard, H., 2015. Removal of lead(II) from aqueous solution using modified palygorskite, contribution of inverse gas chromatography. *J. Chromatogr. A* 1408, 207–216. <https://doi.org/10.1016/j.chroma.2015.07.011>.
- Bouna, L., Rhouta, B., Amjoud, M., Maury, F., Lafont, M.-C., Jada, A., Senocq, F., Daoudi, L., 2011. Synthesis, characterization and photocatalytic activity of TiO_2 supported natural palygorskite microfibers. *Appl. Clay Sci.* 52, 301–311. <https://doi.org/10.1016/j.clay.2011.03.009>.
- Bouna, L., Rhouta, B., Daoudi, L., Maury, F., Amjoud, M., Senocq, F., Lafont, M.C., Jada, A., Ait Aghzzaf, A., 2012. Mineralogical and physico-chemical characterizations of ferruginous beidellite-rich clay from Agadir Basin (Morocco). *Clay Clay Miner.* 60, 278–290. <https://doi.org/10.1346/CCMN.2012.0600305>.
- Caixia, F., Guoguo, L., Pinhong, R., Yan, W., Xianshun, H., Deliang, L., 2014. Effect of photo-corrosion of Ag_2CO_3 on visible light photocatalytic activity of two kinds of $\text{Ag}_2\text{CO}_3/\text{TiO}_2$ prepared from different precursors. *Appl. Catal. B Environ.* 158–159, 224–232.
- Carine Crystallography 3.1 software, 1998. More details on the web site: <http://carine.crystallography.pagesperso-orange.fr/index.html>.
- Carp, O., Huisman, C.L., Reller, A., 2004. Photoinduced reactivity of titanium dioxide. *Prog. Solid State Chem.* 32, 33–177. <https://doi.org/10.1016/j.progsolidstchem.2004.08.001>.
- Changlin, Yu, Wei, Longfu, Chen, Jianchao, Xie, Yu, Zhou, Wanqin, Fan, Qizhe, 2014. Enhancing the photocatalytic performance of commercial TiO_2 crystals by coupling with trace narrow-band-gap Ag_2CO_3 . *Ind. Eng. Chem. Res.* 53, 5759–5766. <https://doi.org/10.1021/ie404283d>.
- Darder, M., Matos, C.R.S., Aranda, P., Gouveia, R.F., Ruiz-Hitzky, E., 2017. Bionanocomposite foams based on the assembly of starch and alginate with sepiolite fibrous clay. *Carbohydr. Polym.* 157, 1933–1939. <https://doi.org/10.1016/j.carbpol.2016.11.079>.
- Emam, E., Centi, G., Perathoner, S., Vaccari, A., 2008. Clays as catalysts in petroleum refining industry. *Appl. Clay Sci.* 3, 161–198. [https://doi.org/10.1016/S0169-1317\(98\)00058-1](https://doi.org/10.1016/S0169-1317(98)00058-1).
- Epling, W.S., Hoflund, G.B., Salaita, G.N., 1998. Surface characterization study of the thermal decomposition of Ag_2CO_3 . *J. Phys. Chem. B* 102, 2263–2268.
- Gout, R., Soubies, F., Bouleau, A., Lurde, C., 1974. Influence de la granulométrie et de la cristallinité sur la vitesse de dissolution de l'hématite dans l'acide chlorhydrique. *Chim. ORSTOM, sér. Pédol.* vol. XII, pp. 289–295 n° 34.
- Holtzapffel, T., 1985. Les minéraux argileux: préparation, analyse diffractométrique et détermination. *Soc. Géol. nord* 12, 15–43.
- Ilsouk, M., Raihane, M., Castelvetro, V., Lahcini, M., Bronco, S., Rhouta, B., Bianchi, S., Conzatti, L., 2017. Highly thermostable and crystalline poly(butylene adipate) bionanocomposites prepared by in situ polycondensation with organically modified Moroccan beidellite clay. *Polym. Int.* 66. <https://doi.org/10.1002/pi.5342>.
- Jahani, D., Ameli, A., Saniei, M., Ding, W., Park, C.B., Naguib, H.E., 2015. Characterization of the structure, acoustic property, thermal conductivity, and mechanical property of highly expanded open-cell polycarbonate foams. *Macromol.*

- Mater. Eng. 300, 48–56. <https://doi.org/10.1002/mame.201400125>.
- Kenne Dedzo, G., Pameté Yambou, E., Topet Saheu, M.R., Ngnie, G., Nansou-Njikji, C.P., Detellier, C., Ngameni, E., 2017. Hydrogen evolution reaction at Pd NPs decorated 1:1 clay minerals and application to the electrocatalytic determination of p-nitrophenol. *J. Electroanal. Chem.* 801, 49–56. <https://doi.org/10.1016/j.jelechem.2017.07.030>.
- Koga, N., Yamada, S., Kimura, T., 2013. Thermal decomposition of silver carbonate: phenomenology and physicochemical kinetics. *J. Phys. Chem. C* 117, 326–336. [dx.doi.org https://doi.org/10.1021/jp309655s](https://doi.org/10.1021/jp309655s).
- Lakbita, O., Rhouta, B., Maury, F., Senocq, F., Amjoud, M., Jada, A., 2016. Supported photocatalyst based on CuO – TiO₂/palygorskite nanocomposite material for wastewater treatment. *J. Colloid Sci. Biotechnol.* 5, 1–7. <https://doi.org/10.1166/jcsb.2016.1150>.
- Lakbita, O., Rhouta, B., Maury, F., Senocq, F., Amjoud, M., Daoudi, L., 2019. Influence of the crystal structure of Ag₂CO₃ on the photocatalytic activity under visible light of Ag₂CO₃-Palygorskite nanocomposite material. *Appl. Surf. Sci.* 464, 205–211. <https://doi.org/10.1016/j.apsusc.2018.09.053>.
- Laufer, G., Kirkland, C., Cain, A.A., Grunlan, J.C., 2012. Clay-chitosan nanobrick walls: completely renewable gas barrier and flame-retardant nanocoatings. *ACS Appl. Mater. Interfaces* 4, 1643–1649. <https://doi.org/10.1021/am2017915>.
- Liu, X., Wang, R., 2017. Effective removal of hydrogen sulfide using 4A molecular sieve zeolite synthesized from attapulgite. *J. Hazard. Mater.* 326, 157–164. <https://doi.org/10.1016/j.jhazmat.2016.12.030>.
- Masse, R., Guitel, J.C., Durif, A., 1979. Structure du carbonate d'argent. *Acta Crystallogr. Sect. B Struct. Crystallogr. Cryst. Chem.* 35, 1428–1429.
- Michau, A., Maury, F., Schuster, F., Boichot, R., Pons, M., 2017. Evidence for a metastable phase as a tracer in DLI-MOCVD chromium hard coatings usable in high temperature environment. *Appl. Surf. Sci.* 422, 198–206. <https://doi.org/10.1016/j.apsusc.2017.05.253>.
- Msaadi, R., Ammar, S., Chehimi, M.M., Yagci, Y., 2017. Diazonium-based ion-imprinted polymer/clay nanocomposite for the selective extraction of lead (II) ions in aqueous media. *Eur. Polym. J.* 89, 367–380. <https://doi.org/10.1016/j.eurpolymj.2017.02.029>.
- Mudrinić, T., Mojović, Z., Milutinović-Nikolić, A., Mojović, M., Žunić, M., Vukelić, N., Jovanović, D., 2015. Electrochemical activity of iron in acid treated bentonite and influence of added nickel. *Appl. Surf. Sci.* 353, 1037–1045. <https://doi.org/10.1016/j.apsusc.2015.07.054>.
- Nagy, D., Vergette, J.B., Connolly, J.P., 1971. Differential thermal analysis studies on Ag₂CO₃. *Can. J. Chem.* 49, 3986–3993.
- Norby, P., Dinnebieer, R., Fitch, A.N., 2002. Decomposition of silver carbonate; the crystal structure of two high-temperature modifications of Ag₂CO₃. *Inorg. Chem.* 41, 3628–3637.
- Pérez-Carvajal, J., Aranda, P., Obregón, S., Colón, G., Ruiz-Hitzky, E., 2016. TiO₂-clay based nanoarchitectures for enhanced photocatalytic hydrogen production. *Microporous Mesoporous Mater.* 222, 120–127. <https://doi.org/10.1016/j.micromeso.2015.10.007>.
- Praneeth, N.V.S., Paria, S., 2017. Clay-semiconductor nanocomposites for photocatalytic applications. In: Sen, Tushar Kanti (Ed.), *Clay Minerals: Properties, Occurrence and Uses*. Nova Science Publishers, Rourkela, Odisha, India, pp. 144–184 (Chapter 5).
- Rahman, H.M., Kennedy, M., Löhr, S., Dewhurst, D.N., 2017. Clay-organic association as a control on hydrocarbon generation in shale. *Org. Geochem.* 105, 42–55. <https://doi.org/10.1016/j.orggeochem.2017.01.011>.
- Rhouta, B., Zatile, E., Bouna, L., Lakbita, O., Maury, F., Daoudi, L., Lafont, M.C., Amjoud, M., Senocq, F., Jada, A., Ait Aghzzaf, A., 2013. Comprehensive physicochemical study of dioctahedral palygorskite-rich clay from Marrakech High Atlas (Morocco). *Phys. Chem. Miner.* 40, 411–424. <https://doi.org/10.1007/s00269-013-0579-3>.
- Roque-Ruiz, J.H., Cabrera-Ontiveros, E.A., Torres-Pérez, J., Reyes-López, S.Y., 2016. Preparation of PCL/clay and PVA/clay electrospun fibers for Cadmium (Cd²⁺), Chromium (Cr³⁺), Copper (Cu²⁺) and Lead (Pb²⁺) removal from water. *Water Air Soil Pollut.* 227. <https://doi.org/10.1007/s11270-016-2990-0>.
- Roy, A., Butola, B.S., Joshi, M., 2017. Synthesis, characterization and antibacterial properties of novel nano-silver loaded acid activated montmorillonite. *Appl. Clay Sci.* 146, 278–285. <https://doi.org/10.1016/j.clay.2017.05.043>.
- Sawada, Y., Manabe, K., 1991. Thermal decomposition of silver carbonate. *J. Therm. Anal.* 37, 1657–1663.
- Sawada, Y., Mizutani, N., Kato, M., 1989a. Thermal decomposition of silver carbonate. *Thermochim. Acta* 143, 319–324. [https://doi.org/10.1016/0040-6031\(89\)85070-1](https://doi.org/10.1016/0040-6031(89)85070-1).
- Sawada, Y., Mizutani, N., Kato, M., 1989b. Thermal decomposition of silver carbonate Part III. High temperature X-ray diffraction analysis. *Thermochim. Acta* 146, 177–185. [https://doi.org/10.1016/0040-6031\(89\)87087-X](https://doi.org/10.1016/0040-6031(89)87087-X).
- Sawada, Y., Watanabe, N., Henmi, H., Mizutani, N., Kato, M., 1989c. Thermal decomposition of silver carbonate. *Thermochim. Acta* 138, 257–265. [https://doi.org/10.1016/0040-6031\(89\)87262-4](https://doi.org/10.1016/0040-6031(89)87262-4).
- Sawada, Y., Kanou, N., Mizutani, N., 1991. Thermal decomposition of silver carbonate. Part 4. High pressure differential thermal analysis under an atmosphere of carbon dioxide. *Thermochim. Acta* 183, 279–287. [https://doi.org/10.1016/0040-6031\(91\)80464-T](https://doi.org/10.1016/0040-6031(91)80464-T).
- Seidell, Atherton, Linke, William F., 1919. *Solubilities of Inorganic and Organic Compounds*, 2nd ed. D. Van Nostrand Company, New York City, pp. 605.
- Tominaga, M., Oniki, Y., Mochida, S., Kasatani, K., Tani, S., Suzuki, Y., Kawamata, J., 2016. Clay-organic hybrid films exhibiting reversible fluorescent color switching induced by swelling and drying of a clay mineral. *J. Phys. Chem. C* 120, 23813–23822. <https://doi.org/10.1021/acs.jpcc.6b07537>.
- Wenjun, F., Ping, W., Bing, Y., Fengling, Y., Dapeng, L., Zhi, Z., 2015. Ag₃PO₄/Ag₂CO₃ p–n heterojunction composites with enhanced photocatalytic activity under visible light. *Chin. J. Catal.* 36, 2186–2193.
- Xu, H., Zhu, J., Song, Y., Zhu, T., Zhao, W., Song, Y., Da, Z., Liu, C., Li, H., 2015. Fabrication of AgX-loaded Ag₂CO₃ (X = Cl, I) composite and their efficient visible-light-driven photocatalytic activity. *J. Alloys Compounds* 622, 347–357. <https://doi.org/10.1016/j.jallcom.2014.09.148>.
- Yang, Y., Zhang, G., 2012. Preparation and photocatalytic properties of visible light driven Ag\AgBr/attapulgite nanocomposite. *Appl. Clay Sci.* 67–68, 11–17. <https://doi.org/10.1016/j.clay.2012.06.013>.